Magnetic-coupled phase anomaly in mixed-phase $BiFeO_3$ thin films

Yen-Chin Huang (黃彥欽), Yi-De Liou (劉懿德), Heng-Jui Liu (劉恆睿), Hsin-Hua Lee (李欣樺), Yi-Chun Chen (陳宜君), and Ying-Hao Chu (朱英豪)

Citation: APL Materials **5**, 086112 (2017);
View online: https://doi.org/10.1063/1.4990138
View Table of Contents: http://aip.scitation.org/toc/apm/5/8
Published by the American Institute of Physics

Magnetic-coupled phase anomaly in mixed-phase $BiFeO_3$ thin films

Yen-Chin Huang (黃彥欽),[1] Yi-De Liou (劉懿德),[1] Heng-Jui Liu (劉恆睿),[2] Hsin-Hua Lee (李欣樺),[1] Yi-Chun Chen (陳宜君),[1,a] and Ying-Hao Chu (朱英豪)[3,4]

[1]*Department of Physics, National Cheng Kung University, Tainan 70101, Taiwan*
[2]*Department of Materials Science and Engineering, National Chung Hsing University, Taichung 40227, Taiwan*
[3]*Department of Materials Science and Engineering, National Chiao Tung University, Hsinchu 30010, Taiwan*
[4]*Institute of Physics, Academia Sinica, Taipei 11529, Taiwan*

(Received 14 June 2017; accepted 15 August 2017; published online 30 August 2017)

The rich phase diagram of rhombohedral (R)-like and tetragonal (T)-like monoclinic polymorph in strained $BiFeO_3$ (BFO) films brings on various functionalities. Finding correlations of physical ordering parameters in this system is generally difficult because T-like and R-like phases are undistinguishable in many aspects. In this study, the magnetic-coupled structural transitions of the mixed-phase BFO at low temperatures were investigated by atomic force microscopy (AFM), X-ray diffraction (XRD), and Raman spectroscopy. To resolve the complexity resulted from the similarity between T-like and R-like phases, we analyzed the Raman spectra on a micro-scale region with various T/R ratios, which is *in situ* manipulated by an AFM tip carrying a dc bias. Phonons of T-like and R-like phases were thus successfully separated. Based on temperature-dependent XRD and resolved Raman spectra, we observed two isostructural transitions at around 225 K and 150 K, and they are strongly correlated with the magnetic ordering in the mixed-phase BFO film. Moreover, through the effective spin-lattice coupling, the evolution of the T/R polymorph is changed by the magnetic cooling process at low temperatures. This study provides a pathway to modulate phonon behaviors by magnetic fields in a highly strained system. [http://dx.doi.org/10.1063/1.4990138]

$BiFeO_3$ (BFO) is a well-known multiferroic material with both ferroelectric (T_C = 1103 K) and G-type antiferromagnetic (T_N = 643 K) orderings at room temperature.[1–4] It has attracted much attention because of its potential for practical applications of controlling magnetism by electricity. Due to the development of thin film growth engineering, rich BFO phase diagrams with unique physical properties have been observed.[4–7] Among those, the most notable system is the morphotrophic phase boundary (MPB), which is a polymorph containing the distorted tetragonal-like (T-like) phase and the distorted rhombohedral-like (R-like) phase, formed in the highly strained BFO thin film grown on the $LaAlO_3$ (LAO) substrate (strain ~ −4.5%).[5,8–10] The R-like phase here is also reported as S',[11,12] M_R,[13] or M_I[14,15] phase in recent studies. T-like BFO (c/a ~ 1.25) is of M_C monoclinic structure (*Cm* symmetry) with ferroelectric polarization along the $[\upsilon 0 \nu]_{pc}$ axis, while R-like BFO (c/a ~ 1.09) is of M_A monoclinic structure (*Cc* symmetry) with ferroelectric polarization along the $[\upsilon\upsilon\nu]_{pc}$ axis, where the suffix pc denotes the perovskite pseudo cubic lattice.[11,14–22] Many intriguing properties have been found in the mixed-phase BFO, such as the giant piezoelectricity,[23] the emergent ferromagnetism,[16] the multiflexo-effect,[24] the persistent photoconductivity,[25] and the shape-memory effect.[26] These various properties originate from intermediate states between normal tetragonal and

[a]E-mail: ycchen93@mail.ncku.edu.tw

rhombohedral BFO crystal structures, so the knowledge of phase manipulation in highly strained BFO will be the key step. In mixed-phase BFO, the crystal structure, the ferroelectricity, or the magnetism has been found tunable by electric fields[5,8,23,27] or mechanical forces.[28] For the temperature variable, the efforts of previous studies have been made on the evolution of the T-like BFO above or near room temperature;[12,13,15,29–33] for example, a structural transformation of T-like BFO around 400 K accompanied with the change of ferroelectricity has been widely discussed.[12,13,15,29–34] By contrast, in the strained BFO film, only little information about transitions of ordering parameters below room temperature was found.[31,34] The lower symmetry at low temperatures is accompanied with more complexity in such a mixed-phase system, and systematic ways to identify properties of individual phases are required. In traditional rhombohedral BFO (R3c symmetry), the spin reorientation transition has been reported at around 140 K and 200 K,[35–37] which comes along with enhanced electron-phonon and dynamical spin-lattice interactions.[38] Therefore, it is reasonable to expect that physical ordering parameters in mixed-phase BFO will also transform at low temperatures, and their correlated behaviors are yet to be investigated.

Here, in order to disentangle the similarity of T-like and R-like phases, we studied the evolution of mixed-phase BFO by the *in situ* Raman scattering combined with the atomic force microscope (AFM), which effectively separated phonons of T-like and R-like BFO. Based on the temperature-dependent x-ray diffraction (XRD) and Raman spectrum, we can reveal there are two isostructural transitions below room temperature, and the phase evolutions are correlated with the magnetic ordering. Noteworthily, under the influence of external magnetic fields, the BFO polymorph will have anomalous change of phonon behaviors.

The mixed-phase $BiFeO_3$ (BFO) films of 100 nm thickness were grown on $LaAlO_3$ (LAO) (001) substrates buffered with $LaNiO_3$ (LNO) bottom electrodes by a pulsed laser deposition (PLD) technique. Morphology and ferroelectric domain structures were measured by a commercial atomic force microscope (AFM, CPII, Veeco). An ac voltage of 1 V at a frequency of 6.39 kHz was applied to drive the ferroelectric sample through a Pt–Ir coated tip of force constant 7 N/m, and the piezoresponse force microscopy (PFM) signals were then collected by the same tip. The phonon behaviors were investigated using a backscattering confocal microscope combined with a spectrometer (iHR550, Horiba Jobin Yvon), and the excited source is 532 nm solid state laser. A 100× objective lens (NA = 0.95) was used for focusing the laser to the spot size about 3 μm^2 and collecting scattering lights, and a long working distance 50× objective lens (NA = 0.5) was used in a liquid N_2 cryostat based temperature-dependent Raman measurements. The Raman spectra resolution is about 0.74 cm^{-1}. A commercial x-ray diffractometer (D8 Discover, Bruker) with Cu Kα1 radiation (λ = 1.5406 Å) was used to record the temperature-dependent XRD patterns, and the precision to estimate the lattice constant is in the order of 10^{-5} Å. The magnetic moments of samples were detected by a SQUID system (MPMS 3, Quantum Design) in zero-field cooling (ZFC) and field cooling (FC) modes (magnetic field ~ 2000 Oe).

The typical topography of the mixed-phase BFO thin film has stripe-like regions embedded in the flat matrix [Fig. S1(a) of the supplementary material]. By changing the azimuthal angle between the scanning cantilever and the BFO $[010]_{pc}$ axis in the PFM measurements, as shown in Fig. S1, we can find that in-plane polarizations of the periodic long domains on the flat matrix lie along $\langle 100\rangle_{pc}$, and those of the loop-circled domains on the stripe-like regions lie along $\langle 110\rangle_{pc}$. The ferroelectric easy axis reveals that the flat regions are the T-like phase with *Cm* symmetry, while the stripe-like regions are the R-like phase with *Cc* symmetry. According to the group theory, the Γ-point phonon modes of *Cm* and *Cc* symmetry are 15*A*' + 12*A*" and 13*A*' + 14*A*", respectively.[10] It is difficult to distinguish these two phases in the Raman spectra because of the large number of phonon modes with close frequencies in the mixed-phase BFO. To solve this problem, considering that the phase transformation of the highly strained BFO can be manipulated by electric fields,[5,8,23,27] we combined a Raman microscope and the AFM system to test the sample, as illustrated in the schematic of Fig. 1(a). The as-grown mixed-phase regions were locally switched to a pure T-like BFO matrix by the scanning AFM tip carrying a dc bias. The switched square is 5 × 5 μm^2 in Fig. 1, which is about eight times larger than the spot size of laser. Again, the switched area is confirmed as the T-like phase by the character of periodic long domain structures (Fig. S2 of the supplementary material). Comparing the *in situ* Raman results before and after electric-driven phase transformation in the same

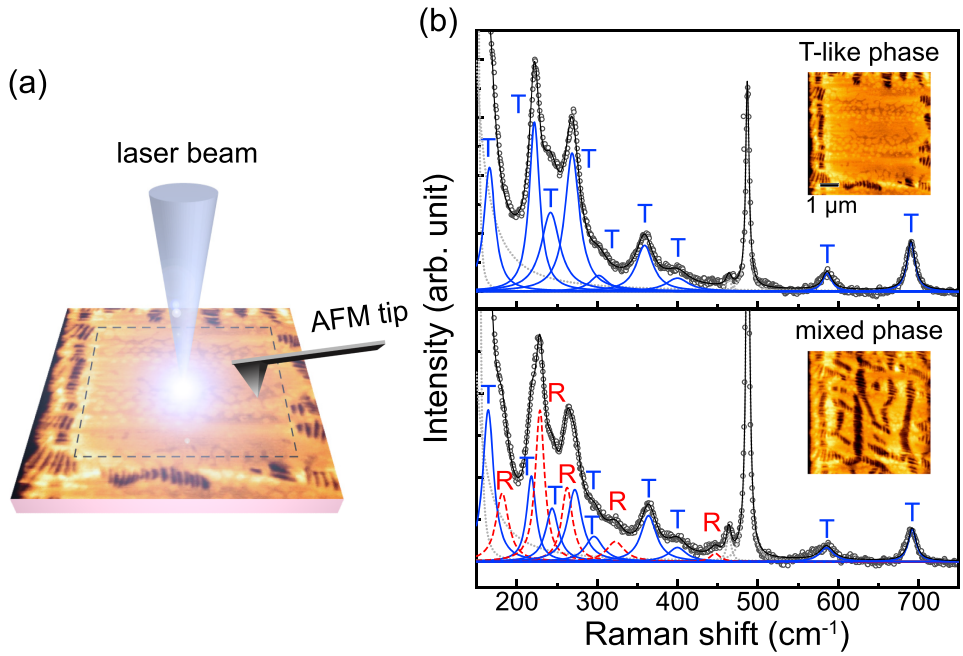

FIG. 1. (a) Schematic representation of the Raman microscope equipped with the AFM. The size switched by the AFM tip is $5 \times 5\,\mu m^2$. (b) Raman spectra and corresponding topographic images of the T-like phase BFO (top panel) and mixed-phase BFO (bottom panel). Blue solid lines and red dashed lines represent fitted phonons of T-like phase and R-like phase, respectively. Gray dotted lines are phonon modes of LAO substrate.

region, we assign the Raman phonons in the top spectrum of Fig. 1(b) to the T-like phase and those only existing in the bottom spectrum of Fig. 1(b) to the R-like phase. Based on this method, phonons of different phases are separated. The resolved phonon assignments are summarized in Table I, where the experimental phonon frequencies are also satisfied with previous observations in strained BFO films.[8,10,13]

We used the temperature-dependent XRD and Raman spectroscopy to study phase evolutions of the mixed-phase BFO. Figure 2(a) shows the XRD data, where the pseudo cubic *c*-axis lattice constants of the T-like phase, the R-like phase and the LAO substrate can be derived from their pseudo cubic (002) peaks, and the results are plotted in Figs. 2(b)–2(d). The *c*-axis lattice constant of the T-like phase has a discontinuous increase around 225 K [Fig. 2(b)] while the c-axis lattice constant of the R-like phase has different temperature dependence above and below 150 K [Fig. 2(c)]. By contrast, LAO only shows monotonic lattice expansion with temperature [Fig. 2(d)]. Accordingly, 225 K and 150 K are expected to be the crystal phase transition temperatures of T-like and R-like phases, respectively. In addition, temperature-dependent Raman spectra supported the phase transitions shown in XRD results, with some Raman phonons significantly changing intensities at similar temperatures (Fig. S3 of the supplementary material). Because temperature dependent Raman spectra reveal no observable changes in crystal symmetry, the structural transitions shown in XRD results should belong to isostructural phase transitions.

Besides the increased phonon numbers, there are abnormal blue shifts of low-frequency Raman peaks around 250 K and 100 K [upper panel of Fig. 3(a)]. Phonons are sensitive to the structure distortion, so these shifts are directly related to the phase transitions observed in XRD. The fitted phonon frequencies in Fig. 3(b) indicate that the blue shifts are contributed from the anomalies of both T-like and R-like phonons at 226 cm^{-1} and 231 cm^{-1}, respectively. The structures of T-like and R-like phases are coupled through the interface strain. Although the transitions of c-axis lattice constants of two phases seem independent in XRD results, the Raman shifts in Fig. 3(b) show that the strain from one phase transformation could result in the distortion of another phase. Figure 3(c) shows the magnetic moments (m) as a function of temperatures under ZFC and FC process. The increased magnetic moments with decreasing temperature correspond with a fundamental trend of

TABLE I. Room-temperature phonon frequencies of T-like phase and R-like phase in this study and the comparison with previous studies (unit: cm^{-1}).

Our study		70 nm	100 nm	100 nm
T	R	BFO/LAO[a]	BFO/LAO[b]	BFO/LAO[c]
138		147	146	
164				
	182			
218		228	220	225
	229		227	
244			242	
	262		266	
272		269	273	266
296				
	323		321	
364		367	368	359
400				
	447			
586		587	587	589
692		691	691	685

[a]Reference 8.
[b]Reference 10.
[c]Reference 13.

collective magnetism. The splitting of ZFC and FC curves around room temperature represents the character of spin-glass transition,[39] and an inflexion point in the FC curve around 100 K indicates another transformation of the magnetic ordering. These two magnetic transition temperatures are close to those of the isostructural transitions, which suggest the changes of magnetic ordering in this system are related to the structure transformations. It is worth noting that different thermal expansion rates of T-like and R-like phases near the isostructural transition temperatures, as shown in Figs. 2(b) and 2(c), result in the variation of interfacial strain during the cooling process. The strain effects can cause the antiferrodistortive (AFD) octahedral rotations[40] and thus change the spin coupling strength in the mixed-phase system. Based on Figs. 2 and 3(c), the discrepancy between the transition temperatures of crystal structures and magnetic orderings are within 50 K.

Further examination was performed by temperature-dependent Raman measurement under magnetic fields. The anomalous phonon shifts around 100 K and 250 K disappear when an external vertical

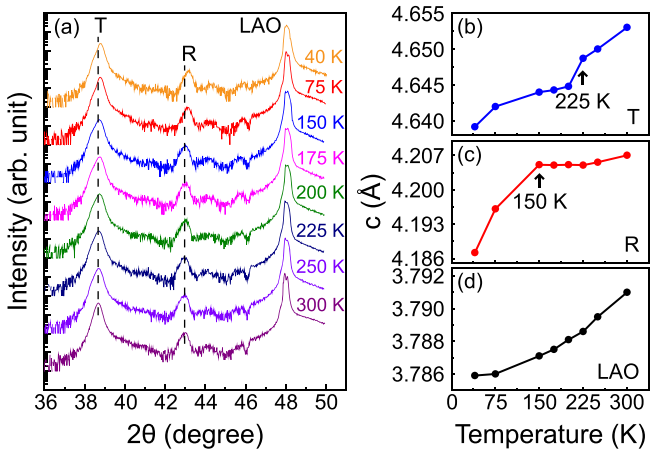

FIG. 2. (a) The pseudo cubic (002) XRD peaks of T-like phase, R-like phase, and LAO substrate as a function of temperature. The calculated pseudo cubic *c*-axis lattice constants versus temperature of (b) T-like phase, (c) R-like phase, and (d) LAO substrate.

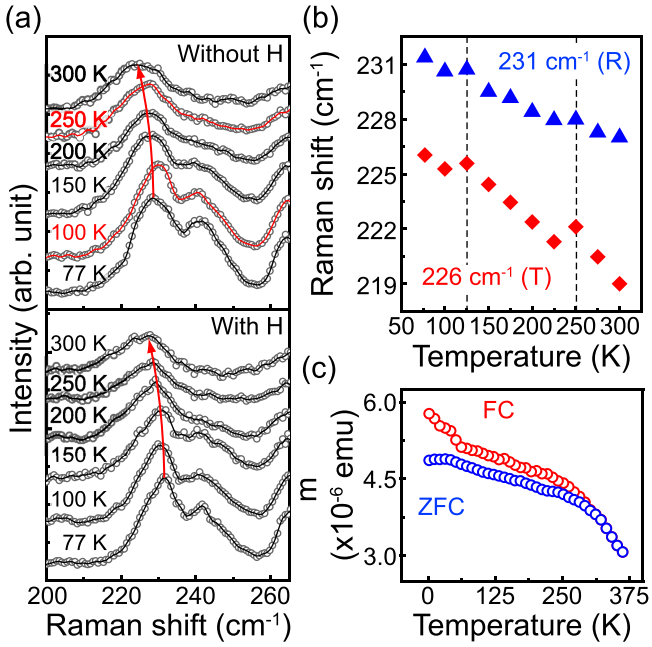

FIG. 3. (a) Raman profiles from 77 K to 300 K without (top) and with (bottom) an external magnetic field. The red colored spectra indicate the anomalous Raman shifts. (b) Temperature-dependent Raman shifts of phonon modes at 226 cm^{-1} and 231 cm^{-1} without external magnetic fields. Dashed lines indicate the temperatures of anomalous Raman shifts. (c) Magnetic moments of mixed-phase BFO versus temperature measured by SQUID.

field of 2000 Oe is applied [lower panel of Fig. 3(a)], and this result reveals that the lattice dynamics is coupled with the spin orientation. The magnetic field-induced phonon shifts can be attributed to two possible mechanisms: spin-phonon interaction and magnetostriction effect. The magnetostrictive coefficient of BFO is only in the order of 10^{-14}–10^{-10},[41] so the maximum strain and the phonon shift ratio ($\Delta\omega/\omega$) caused from the magnetostriction are of the same order, which can hardly be detected in the Raman spectra. Therefore, the possible mechanism left to explain the shifts is the spin-phonon interaction in mixed-phase BFO. Spin-phonon interaction originates from modulating the exchange integrals of neighboring spins by dynamical lattice vibrations, and the lower-frequency phonons are more easily coupled with the magnons. According to above observations of the close temperatures between isostructural and magnetic transitions, also the effect of spin-phonon interaction, we can say that magnetic and crystal structures are effectively coupled in this highly strained system. Note that the crystal symmetry does not change during the magnetic transition, and the similar signature has also been observed in antiferromagnetic-paramagnetic transition of traditional rhombohedral BFO.[42]

Another indication of the strong coupling between the crystal and the magnetism is shown in Fig. 4, where the Raman phonons of T-like and R-like phases are manipulated by external magnetic fields. Figures 4(b) and 4(c) show the variations of phonons at 77 K through cooling processes without and with a vertical magnetic field (~2000 Oe) applied, respectively, and the complete Raman spectra are illustrated in Fig. S4(a). In Fig. 4(c), low-frequency phonons have apparently broader bandwidth compared to those in Fig. 4(b), and the R-like phase phonons show relative decrease in intensity. The bandwidth of low-frequency phonons at 173, 185, 226, 229, 264, and 272 cm^{-1} without/with the magnetic field are 3.4/5.6, 2.8/2.9, 4.0/7.1, 5.4/7.4, 3.0/3.8, and 3.6/6.0 cm^{-1}, respectively. The decreased intensity of R-like phase phonons can be seen by comparing with the nearby T-like phase phonons. Intensity ratios (I_R/I_T) of I(185 cm^{-1})/I(173 cm^{-1}), I(229 cm^{-1})/I(226 cm^{-1}), I(264 cm^{-1})/I(272 cm^{-1}), I(516 cm^{-1})/I(595 cm^{-1}), I(551 cm^{-1})/I(595 cm^{-1}), and I(676 cm^{-1})/I(694 cm^{-1}) without the magnetic field are 0.2, 1.1, 0.5, 0.6, 0.1, and 0.2, and intensity ratios in the magnetic field are 0.1, 0.9, 0.4, 0.3, 0, and 0, respectively. By contrast, the magnetic-dependent phonon variations are not observed at room temperature [Fig. S4(b) of the supplementary material]. These results indicate that the low-temperature crystal structures of mixed phases are affected by the magnetic-cooling

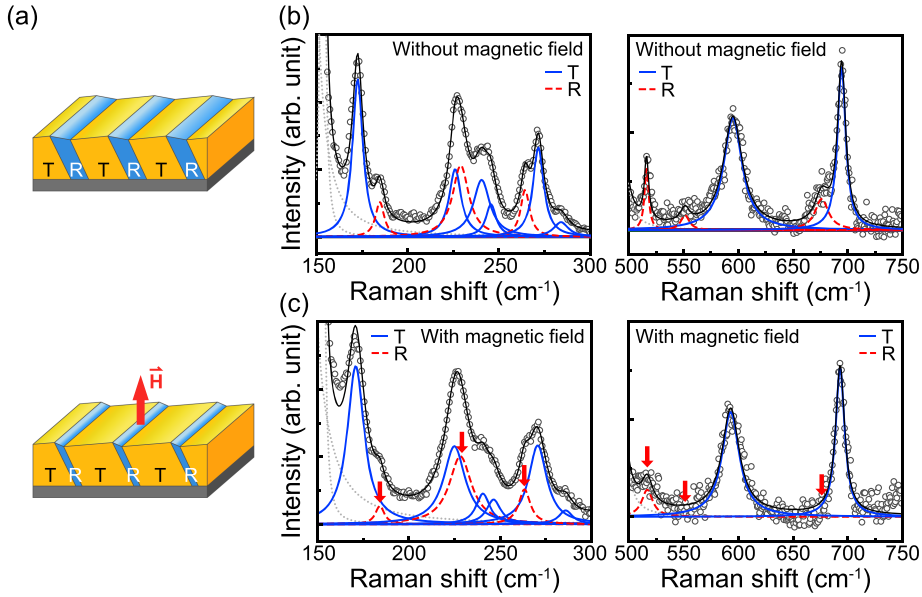

FIG. 4. (a) Schematic diagrams of manipulating the T/R BFO ratio by the magnetic cooling process. (b) and (c) are phonon evolutions with and without an external vertical magnetic field during the cooling process, respectively. Arrows show the decline of phonon intensities. Blue solid lines and red dashed lines represent phonons of T-like and R-like phase, respectively.

history. Due to the small energy difference between metastable phases in the polymorph, even though the external magnetic field only provides small perturbation in the system energy, the phase evolution will choose a similar but different path to another equilibrium state. According to the variations in the Raman spectra, the possible intermediate states under the magnetic-cooling process are distorted crystals or the T/R ratio-changed combinations, as schematically shown in Fig. 4(a).

In summary, our study reveals the magnetic-modulated phase anomaly in mixed-phase BFO at low temperature. By combining AFM and Raman spectroscopy, we successfully distinguish Raman phonons of the T-like and R-like BFO. Two isostructural phase transitions below room temperature are observed: one is the T-like phase transition around 225 K, and the other is the R-like phase transition around 150 K. In addition, the lattice dynamics are coupled with the magnetic ordering. It is interesting to notice that phonon behaviors in mixed-phase BFO change apparently under different magnetic cooling process. The effective spin-lattice coupling in strained BFO provides the opportunity to control phonon-mediated physical properties by magnetic fields.

See supplementary material for the AFM topography and rotated mixed-phase and pure T-like phase PFM images, temperature dependent Raman spectra of mixed-phase BFO, and the comparison of Raman spectra with and without the magnetic field at 77 K and 300 K, respectively.

This work is supported by Ministry of Science and Technology, R.O.C. through the Project No. MOST 105–2112-M-006-001-MY3.

[1] G. A. Smolenskii and I. E. Chupis, Sov. Phys. Usp. **25**, 475 (1982).
[2] J. Wang, J. B. Neaton, H. Zheng, V. Nagarajan, S. B. Ogale, B. Liu, D. Viehland, V. Vaithyanathan, D. G. Schlom, U. V. Waghmare, N. A. Spaldin, K. M. Rabe, M. Wuttig, and R. Ramesh, Science **299**, 1719 (2003).
[3] R. Ramesh and N. A. Spaldin, Nat. Mater. **6**, 21 (2007).
[4] G. Catalan and J. F. Scott, Adv. Mater. **21**, 2463 (2009).
[5] R. J. Zeches, M. D. Rossell, J. X. Zhang, A. J. Hatt, Q. He, C. H. Yang, A. Kumar, C. H. Wang, A. Melville, C. Adamo, G. Sheng, Y. H. Chu, J. F. Ihlefeld, R. Erni, C. Ederer, V. Gopalan, L. Q. Chen, D. G. Schlom, N. A. Spaldin, L. W. Martin, and R. Ramesh, Science **326**, 977 (2009).
[6] I. C. Infante, S. Lisenkov, B. Dupé, M. Bibes, S. Fusil, E. Jacquet, G. Geneste, S. Petit, A. Courtial, J. Juraszek, L. Bellaiche, A. Barthélémy, and B. Dkhil, Phys. Rev. Lett. **105**, 057601 (2010).
[7] D. Sando, A. Barthélémy, and M. Bibes, J. Phys.: Condens. Matter **26**, 473201 (2014).
[8] D. Mazumdar, V. Shelke, M. Iliev, S. Jesse, A. Kumar, S. V. Kalinin, A. P. Baddorf, and A. Gupta, Nano Lett. **10**, 2555 (2010).

[9] B. Dupé, I. C. Infante, G. Geneste, P. E. Janolin, M. Bibes, A. Barthélémy, S. Lisenkov, L. Bellaiche, S. Ravy, and B. Dkhil, Phys. Rev. B **81**, 144128 (2010).
[10] M. N. Iliev, M. V. Abrashev, D. Mazumdar, V. Shelke, and A. Gupta, Phys. Rev. B **82**, 014107 (2010).
[11] C. Beekman, W. Siemons, T. Z. Ward, M. Chi, J. Howe, M. D. Biegalski, N. Balke, P. Maksymovych, A. K. Farrar, J. B. Romero, P. Gao, X. Q. Pan, D. A. Tenne, and H. M. Christen, Adv. Mater. **25**, 5561 (2013).
[12] W. Siemons, C. Beekman, G. J. MacDougall, J. L. Zarestky, S. E. Nagler, and H. M. Christen, J. Phys. D: Appl. Phys. **47**, 034011 (2014).
[13] J. Kreisel, P. Jadhav, O. Chaix-Pluchery, M. Varela, N. Dix, F. Sánchez, and J. Fontcuberta, J. Phys.: Condens. Matter **23**, 342202 (2011).
[14] A. R. Damodaran, C. W. Liang, Q. He, C. Y. Peng, L. Chang, Y. H. Chu, and L. W. Martin, Adv. Mater. **23**, 3170 (2011).
[15] H. J. Liu, C. W. Liang, W.-I. Liang, H. J. Chen, J. C. Yang, C. Y. Peng, G. F. Wang, F. N. Chu, Y. C. Chen, H. Y. Lee, L. Chang, S. J. Lin, and Y. H. Chu, Phys. Rev. B **85**, 014104 (2012).
[16] Q. He, Y. H. Chu, J. T. Heron, S. Y. Yang, W. I. Liang, C. Y. Kuo, H. J. Lin, P. Yu, C. W. Liang, R. J. Zeches, W. C. Kuo, J. Y. Juang, C. T. Chen, E. Arenholz, A. Scholl, and R. Ramesh, Nat. Commun. **2**, 225 (2011).
[17] R. Huang, H. C. Ding, W. I. Liang, Y. C. Gao, X. D. Tang, Q. He, C. G. Duan, Z. Q. Zhu, J. H. Chu, C. A. J. Fisher, T. Hirayama, Y. Ikuhara, and Y. H. Chu, Adv. Funct. Mater. **24**, 793 (2014).
[18] O. Diéguez, O. E. González-Vázquez, J. C. Wojdeł, and J. Íñiguez, Phys. Rev. B **83**, 094105 (2011).
[19] F. Pailloux, M. Couillard, S. Fusil, F. Bruno, W. Saidi, V. Garcia, C. Carrétéro, E. Jacquet, M. Bibes, A. Barthélémy, G. A. Botton, and J. Pacaud, Phys. Rev. B **89**, 104106 (2014).
[20] M. P. Cosgriff, P. Chen, S. S. Lee, H. J. Lee, L. Kuna, K. C. Pitike, L. Louis, W. D. Parker, H. Tajiri, S. M. Nakhmanson, J. Y. Jo, Z. Chen, L. Chen, and P. G. Evans, Adv. Electron. Mater. **2**, 1500204 (2016).
[21] H. M. Christen, J. H. Nam, H. S. Kim, A. J. Hatt, and N. A. Spaldin, Phys. Rev. B **83**, 144107 (2011).
[22] Z. H. Chen, Z. L. Luo, C. W. Huang, Y. J. Qi, P. Yang, L. You, C. S. Hu, T. Wu, J. L. Wang, C. Gao, T. Sritharan, and L. Chen, Adv. Funct. Mater. **21**, 133 (2011).
[23] J. X. Zhang, B. Xiang, Q. He, J. Seidel, R. J. Zeches, P. Yu, S. Y. Yang, C. H. Wang, Y. H. Chu, L. W. Martin, A. M. Minor, and R. Ramesh, Nat. Nanotechnol. **6**, 98 (2011).
[24] J. X. Zhang, R. J. Zeches, Q. He, Y. H. Chu, and R. Ramesh, Nanoscale **4**, 6196 (2012).
[25] A. Bhatnagar, Y. H. Kim, D. Hesse, and M. Alexe, Nano Lett. **14**, 5224 (2014).
[26] J. X. Zhang, X. X. Ke, G. Y. Gou, J. Seidel, B. Xiang, P. Yu, W. I. Liang, A. M. Minor, Y. H. Chu, G. Van Tendeloo, X. B. Ren, and R. Ramesh, Nat. Commun. **4**, 2768 (2013).
[27] Y. C. Chen, Q. He, F. N. Chu, Y. C. Huang, J. W. Chen, W. I. Liang, R. K. Vasudevan, V. Nagarajan, E. Arenholz, S. V. Kalinin, and Y. H. Chu, Adv. Mater. **24**, 3070 (2012).
[28] Y. J. Li, J. J. Wang, J. C. Ye, X. X. Ke, G. Y. Gou, Y. Wei, F. Xue, J. Wang, C. S. Wang, R. C. Peng, X. L. Deng, Y. Yang, X. B. Ren, L. Q. Chen, C. W. Nan, and J. X. Zhang, Adv. Funct. Mater. **25**, 3405 (2015).
[29] K. T. Ko, M. H. Jung, Q. He, J. H. Lee, C. S. Woo, K. Chu, J. Seidel, B. G. Jeon, Y. S. Oh, K. H. Kim, W. I. Liang, H. J. Chen, Y. H. Chu, Y. H. Jeong, R. Ramesh, J. H. Park, and C. H. Yang, Nat. Commun. **2**, 567 (2011).
[30] I. C. Infante, J. Juraszek, S. Fusil, B. Dupé, P. Gemeiner, O. Diéguez, F. Pailloux, S. Jouen, E. Jacquet, G. Geneste, J. Pacaud, J. Íñiguez, L. Bellaiche, A. Barthélémy, B. Dkhil, and M. Bibes, Phys. Rev. Lett. **107**, 237601 (2011).
[31] G. J. MacDougall, H. M. Christen, W. Siemons, M. D. Biegalski, J. L. Zarestky, S. Liang, E. Dagotto, and S. E. Nagler, Phys. Rev. B **85**, 100406 (2012).
[32] W. Siemons, G. J. MacDougall, A. A. Aczel, J. L. Zarestky, M. D. Biegalski, S. Liang, E. Dagotto, S. E. Nagler, and H. M. Christen, Appl. Phys. Lett. **101**, 212901 (2012).
[33] C. Escorihuela-Sayalero, O. Diéguez, and J. Íñiguez, Phys. Rev. Lett. **109**, 247202 (2012).
[34] K. Y. Choi, S. H. Do, P. Lemmens, D. Wulferding, C. S. Woo, J. H. Lee, K. Chu, and C. H. Yang, Phys. Rev. B **84**, 132408 (2011).
[35] M. K. Singh, R. S. Katiyar, and J. F. Scott, J. Phys.: Condens. Matter **20**, 252203 (2008).
[36] J. F. Scott, M. K. Singh, and R. S. Katiyar, J. Phys.: Condens. Matter **20**, 322203 (2008).
[37] P. Rovillain, M. Cazayous, Y. Gallais, A. Sacuto, R. P. S. M. Lobo, D. Lebeugle, and D. Colson, Phys. Rev. B **79**, 180411(R) (2009).
[38] Z. Y. Zhang, Z. M. Jin, Q. F. Pan, Y. Xu, X. Lin, G. H. Ma, and Z. X. Cheng, Appl. Phys. Lett. **104**, 151902 (2014).
[39] S. Nakamura, S. Soeya, N. Ikeda, and M. Tanaka, J. Appl. Phys. **74**, 5652 (1993).
[40] H. Dixit, J. H. Lee, J. T. Krogel, S. Okamoto, and V. R. Cooper, Sci. Rep. **5**, 12969 (2015).
[41] A. Kumar, J. F. Scott, R. Martinez, G. Srinivasan, and R. S. Katiyar, Phys. Status Solidi A **209**, 1207 (2012).
[42] R. Haumont, J. Kreisel, P. Bouvier, and F. Hippert, Phys. Rev. B **73**, 132101 (2006).